PAPER • OPEN ACCESS

Non-volatile memory storage in tri-layer structures using the intrinsically ferromagnetic semiconductors GdN and DyN

To cite this article: Sam Devese *et al* 2022 *Nano Ex.* **3** 045007

View the article online for updates and enhancements.

**NANO
EXPRESS**

PAPER

Non-volatile memory storage in tri-layer structures using the intrinsically ferromagnetic semiconductors GdN and DyN

Sam Devese[1],[*] ⓘ, Catherine Pot[1] ⓘ, Franck Natali[1] ⓘ, Simon Granville[2] ⓘ, Natalie Plank[1] ⓘ, Ben J Ruck[1], H Joe Trodahl[1] and William Holmes-Hewett[1]

[1] The MacDiarmid Institute for Advanced Materials and Nanotechnology, School of Chemical and Physical Sciences, Victoria University of Wellington, P.O. Box 600, Wellington 6140, New Zealand
[2] The MacDiarmid Institute for Advanced Materials and Nanotechnology, Robinson Research Institute, Victoria University of Wellington, P.O. Box 33436, Petone 5046, New Zealand
[*] Author to whom any correspondence should be addressed.

E-mail: sam.devese@vuw.ac.nz and william.holmes-hewett@vuw.ac.nz

Abstract

We report on the potential use of the intrinsic ferromagnetic rare earth nitride (REN) semiconductors as ferromagnetic electrodes in tunnelling magnetoresistance and giant magnetoresistance device structures for non-volatile memory storage devices. Non-volatile memory elements utilising magnetic materials have been an industry standard for decades. However, the typical metallic ferromagnets and dilute magnetic semiconductors used lack the ability to independently tune the magnetic and electronic properties. In this regard, the rare earth nitride series offer an ultimately tuneable group of materials. Here we have fabricated two tri-layer structures using intrinsically ferromagnetic rare earth nitride semiconductors as the ferromagnetic layers. We have demonstrated both a non-volatile magnetic tunnel junction (MTJ) and an in-plane conduction device using GdN and DyN as the ferromagnetic layers, with a maximum difference in resistive states of ∼1.2% at zero-field. GdN and DyN layers were shown to be sufficiently decoupled and individual magnetic transitions were observed for each ferromagnetic layer.

1. Introduction

There is an intense research and development effort for novel solid state memory devices that is critical for the future of cloud computing and data storage [1–3]. The quest is to balance speed, power, endurance, and cost in order to enable a new paradigm of non-volatile random-access memory (RAM) [4–6]. Several architectures, technologies, and materials for various types of random-access memory, including spin-transfer torque RAM, resistive and/or magnetic RAM, ferroelectric RAM and more have drawn the most attention and have been studied extensively during the past several years.

From a material perspective, metallic ferromagnetic (FM) materials have been historically by far the most common ferromagnetic layers in ambient-temperature memory elements, either in a giant magnetoresistance (GMR) structure [7] or as magnetic tunnel junctions (MTJs). Such devices typically comprise a tri-layer made of two metallic ferromagnetic layers separated by an exchange-blocking (EB) layer, with the resistance of the layered structures depending on the relative orientations of magnetisation, parallel or anti-parallel magnetic alignment, in the FM layers. Such elements are already commonly applied as both memory structures and read heads for magnetic memories, but lack the ability to independently tune the magnetic and electronic properties [4]. In contrast, ferromagnetic semiconductors offer a potential range of new functionalities based on their independently-tuneable carrier concentration and spin polarisation.

Dilute magnetic semiconductors (DMS), a class of materials that combine properties of a semiconductor host with magnetic effects due to an impurity dopant, have shown promise in memory and logic applications

[8, 9], but the dependence of the transition temparure on the density of mobile carriers limit their range of applications [9–12]. In this regard the separation of electronic and magnetic degrees of freedom in the series of intrinsically ferromagnetic rare earth nitride (REN) semiconductors make them ideal candidate materials for non-volatile memory elements at cryogenic temperatures [13–16]. Below we exploit this control to demonstrate two contrasting schemes, magnetic tunnel junctions and in-plane conduction structures to determine the relative magnetisation of the two rare-earth nitride FM layers: the data reading operation.

The RENs form in the face centred cubic rock-salt structure [17–19] with their magnetic properties within the series determined by the filling of the $4f$ shell in the rare earth ion. The wide range of spin and unquenched orbital moments across the series leads to strongly contrasting ferromagnetic moments and coercive fields [20]. In the stoichiometric form they are insulating with N $2p$ valence and RE $5d$ conduction bands. Nitrogen vacancies, each of which adds a mobile electron to the conduction band [21], can be used as convenient electron donors.

The pair GdN and DyN are chosen for the present prototype devices for their contrasting magnetic but similar electronic states. GdN has an electronic configuration $4f^7$ resulting in a magnetic moment of 7 μ_B per Gd ion that resides in the $4f$-shell spin. It is ferromagnetic below ∼70 K and has a small coercive field on the order of 10 mT or less at 5 K [22]. The two additional $4f$ electrons in the Dy^{3+} ion gives DyN a mixed spin/orbit moment of 10 μ_B per ion in the paramagnetic state, falling to ∼5 μ_B under the exchange interaction in the FM state below its ∼30 K Curie temperature [16]. The FM state features a coercive field at 5 K on the order of 100 mT [14], thus forming a suitable hard FM pairing for the softer ferromagnetic GdN. In the present context it is important to note that the end members of the series, LaN and LuN, have empty and filled $4f$ shells respectively, and thus are non-magnetic; in this study we have used LuN and Lu as an insulating and a metallic exchange-blocking layer respectively.

It is worth pointing out that REN-based MTJs have been reported in the past [23, 24], but none of them have demonstrated the non-volatile behaviour characteristic of a memory element. Additionally, here we incorporate RENs into a GMR-style device which also displays retention of its resistive states.

This report describes two contrasting prototype memory device structures based entirely on RE and REN active layers in a common tri-layer structure GdN/EB/DyN (EB—a non-magnetic exchange-blocking layer). The first uses an entirely conventional current perpendicular to plane (CPP) geometry in a GdN/LuN/DyN tri-layer with an insulating EB layer in which the tunnelling magnetoresistance is modulated by the relative magnetic alignments of the two FM layers, as shown in figure 1(a). It is important in this device, with its in series resistances, that the FM layers introduce negligible resistance relative to the tunnel barrier. In this regard, the LuN barrier must be at most very weakly doped, while the FM layers should be more heavily doped.

Though the CPP geometry is very common, there is an advantage in some cases (e.g. superconducting central processors) to investigate low-impedance data reading. Thus the second structure, show in figure 1(b), is a current in-plane (CIP) device, GdN/Lu/DyN, relying on the giant magnetoresistance in the exchange-blocking layer to differentiate between the parallel and anti-parallel magnetic configurations. In this geometry, with the three layers contributing to the resistance in parallel, the FM layers must be insulating, at most weakly doped. Thus it is central to the two devices that the REN films can be doped from metallic to insulating without affecting their magnetisations.

2. Experimental details

All layers were grown in a molecular beam epitaxy (MBE) system with a base pressure of ∼10^{-9} mbar. The FM rare earth nitride layers were grown by evaporating metallic Gd or Dy in an atmosphere of ∼2×10^{-4} mbar of N_2. The differing nature of the two device structures described previously required significantly different growth conditions for their respective EB layers.

The insulating EB layer, ∼8 nm of LuN, was grown by evaporating Lu in an atmosphere of N_2, similar to the FM rare earth nitride layers described above. For the low-impedance GMR device the EB layer is metallic Lu ∼20 nm thick. The conductive EB layer was grown by evaporating Lu at the base pressure of ∼10^{-9} mbar. Each device was simultaneously grown on polished Al_2O_3 and Si substrates, which were held at ambient temperature throughout the growth. A protective layer of ∼40 nm thick AlN or Al is used to protect all the devices from oxidation.

The differing structure between the low-impedance GMR device and high-impedance tunnelling devices result in differing geometries for electrical measurement. Electrical contact was made to the low-impedance GMR devices via Au bottom contacts in a van der Pauw configuration, which were deposited before the device growth. Electrical measurement for the high-impedance tunnelling device comprised vertical transport from a pre-deposited Au layer, though the device in the *caisson* structure, to the metallic Al protective layer, as described in our previous publication [23].
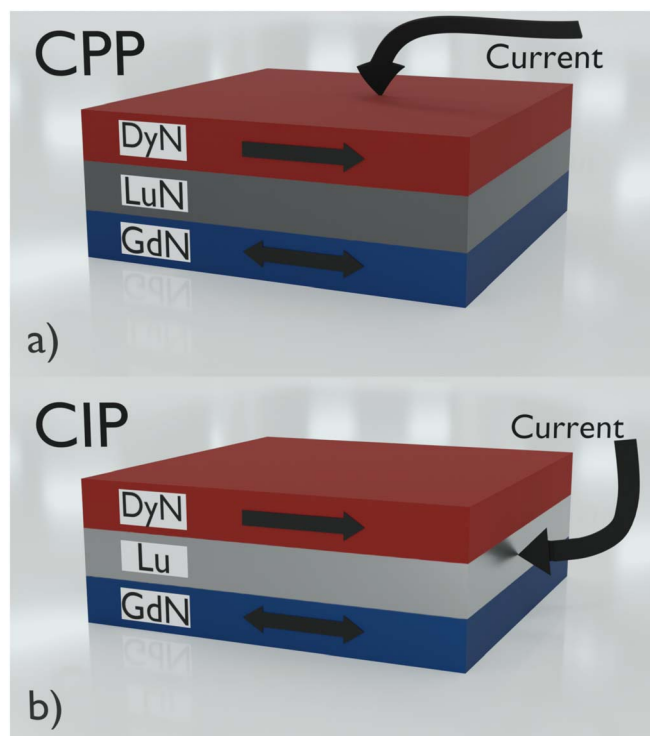
Figure 1. Schematic showing the current flow direction and relative magnetisation (black arrows) of the GdN (blue) and DyN (red) layers. The high resistance magnetic tunnel junction is shown with an insulating LuN barrier (grey) and current perpendicular to plane (a). The low resistance in-plane conduction device is shown with a conductive Lu (silver) exchange-blocking layer (b).
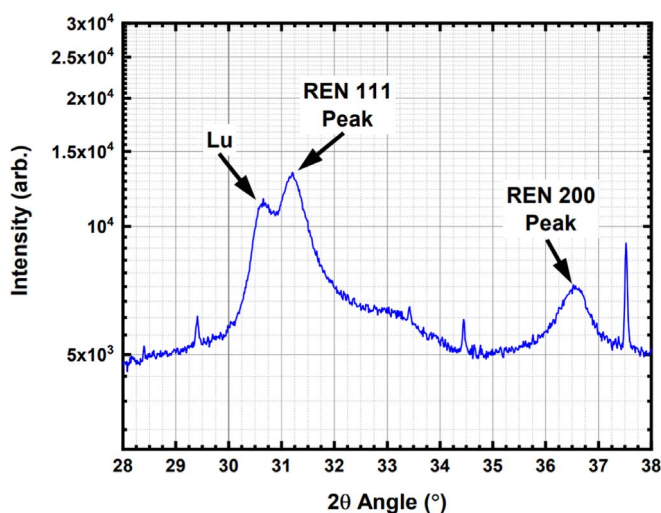

Figure 2. 2θ-θ x-ray diffractogram of a GdN/Lu/DyN thin film heterostructure grown on sapphire substrate. Peaks due to the Lu (002), REN (111), and REN (200) are labelled. The separate contributions in each REN peak due to the polycrystalline GdN and DyN layers are not distinguishable. A sharp peak related to secondary emissions of the Cu x-ray source on the Al_2O_3 substrate (0006) peak is also present at ~37.4°

x-ray diffraction (XRD) was used to characterise the films grown on all substrates using a PAN-alytical X'Pert PRO x-ray diffractometer with Cu K-alpha source. All films showed the characteristic rock-salt REN features, with both 111 and 200 rare earth nitride peaks present in agreement with previously published data for GdN and DyN thin films grown under similar conditions [25, 26]. Figure 2 shows the 2θ-θ XRD scan, highlighting the (111) REN reflection at ~31.2°. Due to their similar lattice constants, the (111) XRD peaks of GdN and DyN layers show strong overlap and cannot be distinguished. This is as expected, with previous XRD measurements on polycrystalline rare earth nitride superlattices also unable to distinguish separate contributions to the REN (111) peak [27–29]. A slight asymmetry in the (200) peak at ~36.4° implies two separate REN contributions,
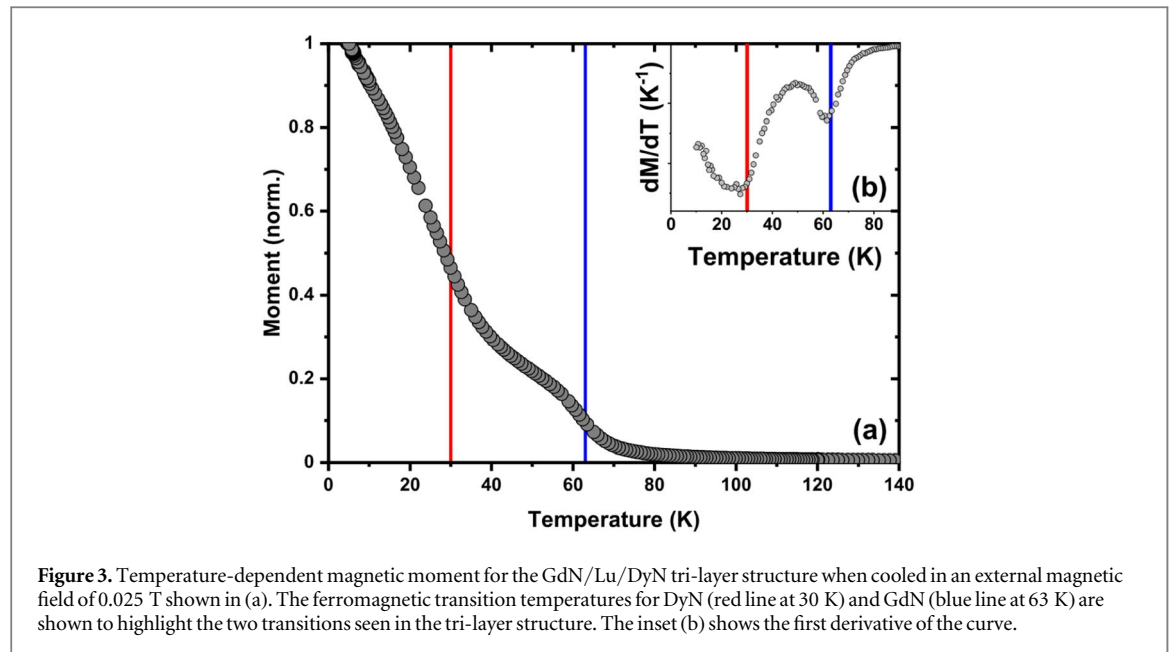
Figure 3. Temperature-dependent magnetic moment for the GdN/Lu/DyN tri-layer structure when cooled in an external magnetic field of 0.025 T shown in (a). The ferromagnetic transition temperatures for DyN (red line at 30 K) and GdN (blue line at 63 K) are shown to highlight the two transitions seen in the tri-layer structure. The inset (b) shows the first derivative of the curve.

however the presence of separate GdN and DyN layers is more clearly demonstrated in the magnetic measurements discussed later in this paper.

In-plane magnetisation measurements were made using a Quantum Design model XL MPMS to obtain temperature- and magnetic field-dependent magnetisation. Electrical transport measurements were made in a Quantum Design Physical Property Measurement System (PPMS) Model 6000.

3. Results and discussion

We begin by discussing the magnetic results in general, followed by a separate discussion of the electronic properties and memory facilities for the high and low impedance devices respectively.

3.1. Magnetic behaviour
The temperature-dependent magnetisation $M(T)$ is shown in figure 3 for the GdN/Lu/DyN tri-layer structure. The first derivative, shown in the inset, highlights the distinct magnetic transitions of GdN near 63 K and DyN near 30 K. The two distinct transitions indicates that the two layers are magnetically isolated from each other by the non-magnetic EB layer, in this case Lu. Similar behaviour was observed for the high impedance device using LuN.

3.2. Electronic behaviour
3.2.1. High-impedance device
The resistance measured for the GdN/LuN/DyN device varies depending on the applied current. This deviation from Ohm's Law signals a tunnelling current [30, 31] and the non-linearity is highlighted in figure 4(a). Linear behaviour was observed at low voltages. However, for voltages above ∼0.1 V it can be seen that the device exhibits non-linear current-voltage characteristics. The temperature-dependent resistance for different applied currents is shown in figure 4(b) and similarly displays this non-linear behaviour. The device has a negative temperature coefficient of resistance with a noticeable peak near 25 K. This feature is commonly attributed to the onset of magnetic order associated with the FM transition in RENs [21, 32]. It is worth noting here that vast majority of the voltage drop in the device is expected over the LuN barrier layer.

The low-field magnetoresistance of this device is shown in figure 5. Here the measurement is with a constant current of 0.5 μA, which is within the non-linear tunnelling regime in figure 4(a). By first sweeping the applied field to 8 T the two FM layers have their magnetisation aligned. This aligned state corresponds to the low-resistance state of the device as the tunnelling current across the barrier is dominated by majority-majority band transport, and thus is facilitated due to the many available states above the Fermi level. Conversely, the high resistance state occurs when the magnetisation of the two FM layers is anti-aligned. To compare the high and low impedance devices, we use R_{AP} and R_P as the resistance values of the device in the anti-parallel and parallel states respectively and represent the magnetoresistance (MR) ratio as:
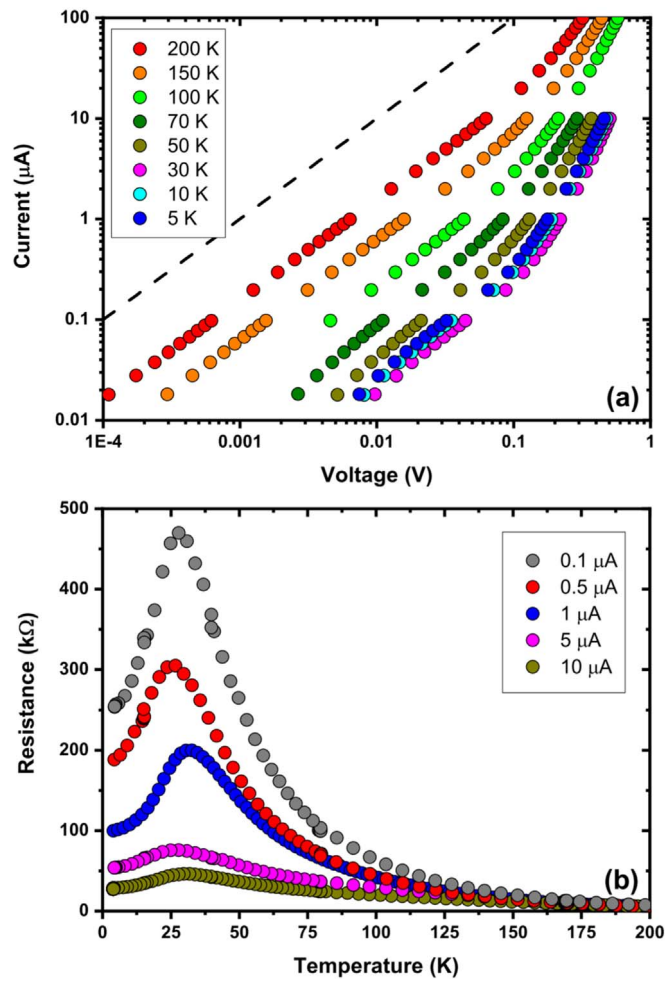
Figure 4. (a) Logarithmic plot of the current-voltage behaviour for the GdN/LuN/DyN magnetic tunnel junction and (b) the temperature-dependent resistance measured at different applied currents. In (a) a linear relationship can be seen at lower voltages, with a non-linear regime developing above voltages of ∼0.1 V. The dashed line is added as a guide to the eye for a gradient of unity.
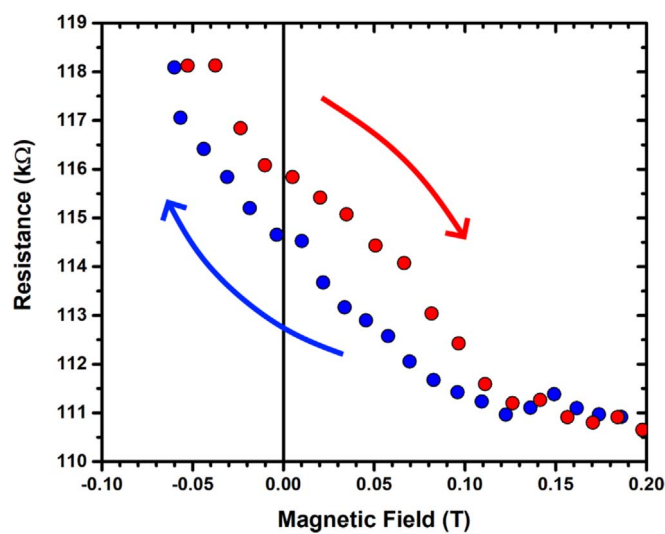

Figure 5. Magnetoresistance plot for the high-impedance DyN/LuN/GdN magnetic tunnel junction with the field being swept from +8 T down to −0.06 T (blue) and then back to +8 T (red). The difference in resistance between the two sweeps at 0 T (black line) is ∼1.2%.
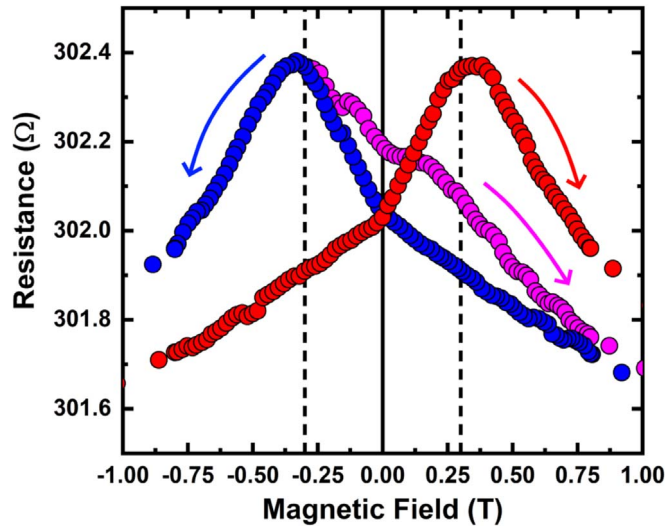
Figure 6. Magnetoresistance plot for the low-impedance DyN/Lu/GdN in-plane conduction device for increasing (red) and decreasing (blue) field sweep directions between $\pm$ 1 T. A minor sweep (purple) shows the magnetoresistance values for increasing magnetic field when the device is taken down to −0.3 T. A solid black line is shown at 0 T to highlight the difference between increasing and decreasing 0 T resistance values for the minor sweep and the dashed black lines indicate $\pm$ 0.3 T near the maximum magnetoresistance.

$$MR = (R_{AP} - R_P)/R_P \qquad\qquad (1)$$

The magnetoresistance at 5 K for this GdN/LuN/DyN device is subsequently found to be 19.2%, using values for R_{AP} and R_P close to 0 T and 8 T respectively. Hysteresis is observed, with resistance dependent on the direction of the magnetic field sweep and a clear peak in resistance at a magnetic field corresponding to the coercive field of GdN $\sim$0.06 T. At this magnetic field, the magnetisation in the GdN layer has switched direction so that the two FM layers have their magnetisation anti-aligned, resulting in a high-resistance state. By sweeping the field to this peak and then reversing the direction of the magnetic field sweep, this high-resistance state is able to be preserved at 0 T. The difference between the high- and low-resistance states of the GdN/LuN/DyN tri-layer at zero-field is $\sim$1.2%.

3.3. Low-impedance device

We now turn to the low-impedance CIP device. The field-dependent magnetoresistance of this device is shown in figure 6 which shows a zoom between $\pm$1 T of a full-field hysteresis loop between $\pm$8 T. The device is thus taken though both parallel and anti-parallel states, corresponding to the peaks in the resistance near $\pm$0.3 T. The magnetoresistance at 5 K was $\sim$0.8%, which is noteworthy for a tri-layer structure, and comparable even to some multi-layered GMR-based devices on the order of 1% [33, 34].

The purple trace in figure 6 shows a measurement where the device was taken from the parallel low-resistance state, to the anti-parallel high-resistance state, and then through zero field. Here we see that the high resistance state is found near −0.3 T and, importantly, that this high resistance state is retained at zero field. The difference in resistive states at zero-field observed here was $\sim$0.04%. While it is noted that the magnetoresistance values presented here for both devices are smaller than expected for typical metallic ferromagnet-based devices, they are on the order of other magnetically controlled ferromagnetic semiconductor-based devices, here with the added demonstration of retention [34–38].

4. Conclusions

We have demonstrated both a non-volatile magnetic tunnel junction and an in-plane conduction device using GdN and DyN as the ferromagnetic layers, with a maximum difference in resistive states of $\sim$1.2% at zero-field. GdN and DyN layers were shown to be sufficiently decoupled and individual magnetic transitions were observed for each ferromagnetic layer. This work serves as clear evidence for the potential of REN materials as ferromagnetic layers in non-volatile cryogenic memory storage devices, opening the door to further structures using these materials in epitaxial or multi-layer devices.

Data availability statement

The data that support the findings of this study are available upon reasonable request from the authors.

ORCID iDs

Sam Devese ⬤ https://orcid.org/0000-0002-4311-1881
Catherine Pot ⬤ https://orcid.org/0000-0001-7970-2344
Franck Natali ⬤ https://orcid.org/0000-0001-5407-1929
Simon Granville ⬤ https://orcid.org/0000-0001-9926-4628
Natalie Plank ⬤ https://orcid.org/0000-0002-9798-9657

References

[1] International Roadmap for Devices and Systems (IRDS^{TM}) 2021 Edition—IEEE IRDS^{TM}
[2] Soloviev I I, Klenov N V, Bakurskiy S V, Kupriyanov M Y, Gudkov A L and Sidorenko A S 2017 *Beilstein J. Nanotechnol.* **8** 2689–710
[3] Linder J and Robinson J W A 2015 *Nat. Phys.* **11** 307–15
[4] Vernik I V, Bol'ginov V V, Bakurskiy S V, Golubov A A, Kupriyanov M Y, Ryazanov V V and Mukhanov O A 2013 *IEEE Trans. Appl. Supercond.* **23** 1701208
[5] Manheimer M A 2015 *IEEE Trans. Appl. Supercond.* **25** 1–4
[6] Ortlepp T and Van Duzer T 2014 *IEEE Trans. Appl. Supercond.* **24** 1–7
[7] Baibich M N, Broto J M, Fert A, Van Dau F N, Petroff F, Etienne P, Creuzet G, Friederich A and Chazelas J 1988 *Phys. Rev. Lett.* **61** 2472–5
[8] Mark S, Dürrenfeld P, Pappert K, Ebel L, Brunner K, Gould C and Molenkamp L W 2011 *Phys. Rev. Lett.* **106** 057204
[9] Dietl T 2010 *Nat. Mater.* **9** 965–74
[10] Gupta A, Zhang R, Kumar P, Kumar V and Kumar A 2020 *Magnetochemistry* **6** 15
[11] Tanaka M and Higo Y 2001 *Phys. Rev. Lett.* **87** 026602
[12] Zhao G, Deng Z and Jin C 2019 *J. Semicond.* **40** 081505
[13] Trodahl H J, Natali F, Ruck B J and Lambrecht W R L 2017 *Phys. Rev.* B **96** 115309
[14] Holmes-Hewett W F, Pot C, Buckley R G, Koo A, Ruck B J, Natali F, Shaib A, Miller J D and Trodahl H J 2020 *Appl. Phys. Lett.* **117** 222409
[15] Plank N O V, Natali F, Galipaud J, Richter J H, Simpson M, Trodahl H J and Ruck B J 2011 *Appl. Phys. Lett.* **98** 112503
[16] Pot C, Holmes-Hewett W F, Ruck B J and Trodahl H J 2021 *Appl. Phys. Lett.* **119** 172406
[17] Granville S, Meyer C, Preston A R H, Ludbrook B M, Ruck B J, Trodahl H J, Paudel T R and Lambrecht W R L 2009 *Phys. Rev.* B **79** 054301
[18] Natali F, Plank N O V, Galipaud J, Ruck B J, Trodahl H J, Semond F, Sorieul S and Hirsch L 2010 *J. Cryst. Growth* **312** 3583–7
[19] Natali F *et al* 2012 *Phys. Status Solidi* C **9** 605–8
[20] Natali F, Ruck B J, Plank N O V, Trodahl H J, Granville S, Meyer C and Lambrecht W R L 2013 *Prog. Mater Sci.* **58** 1316–60
[21] Granville S *et al* 2006 *Phys. Rev.* B **73** 235335
[22] Ludbrook B M, Farrell I L, Kuebel M, Ruck B J, Preston A R H, Trodahl H J, Ranno L, Reeves R J and Durbin S M 2009 *J. Appl. Phys.* **106** 063910
[23] Miller J D, Ullstad F H, Trodahl H J, Ruck B J and Natali F 2020 *Nanotechnology* **31** 235202
[24] Warring H, Trodahl H, Plank N, Natali F, Granville S and Ruck B 2016 *Physical Review Applied* **6** 044002
[25] Shaib A, Natali F, Chan J R, Ullstad F, Holmes-Hewett W F, Miller J D, Ruck B J and Trodahl H J 2020 *Mater. Res. Express* **7** 046404
[26] Azeem M, Ruck B J, Do Le B, Warring H, Trodahl H J, Strickland N M, Koo A, Goian V and Kamba S 2013 *J. Appl. Phys.* **113** 203509
[27] McNulty J F, Anton E M, Ruck B J, Natali F, Warring H, Wilhelm F, Rogalev A, Soares M M, Brookes N B and Trodahl H J 2015 *Phys. Rev.* B **91** 174426
[28] Natali F, Trodahl J, Vézian S, Traverson A, Damilano B and Ruck B 2017 *MRS Advances* **2** 189–94
[29] McNulty J F, Anton E M, Ruck B J, Suzuki M, Mizumaki M and Trodahl H J 2019 *Phys. Rev.* B **100** 094441
[30] Nazarov Y V 1995 *Generalized Ohm's Law Quantum Dynamics of Submicron Structures* ed HA Cerdeira, B Kramer and G Schön (Dordrecht, Netherlands: Springer) pp 687–704
[31] Farooq Khan M, Kim H, Nazir G, Jung S and Eom J 2018 *Nanoscale* **10** 16703–10
[32] Anton E M *et al* 2016 *Phys. Rev.* B **94** 024106
[33] Wang H, Lu C, Chen J, Liu Y, Yuan S L, Cheong S W, Dong S and Liu J M 2019 *Nat. Commun.* **10** 2280
[34] Liu M, Du W, Su H, Zhang H, Liu B, Meng H and Tang X 2021 *NPG Asia Mater.* **13** 1–7
[35] Wang W *et al* 2015 *Nano Lett.* **15** 5261–7
[36] Yau H M, Yan Z B, Chan N Y, Au K, Wong C M, Leung C W, Zhang F Y, Gao X S and Dai J Y 2015 *Sci. Rep.* **5** 12826
[37] Rüster C, Gould C, Jungwirth T, Girgis E, Schott G M, Giraud R, Brunner K, Schmidt G and Molenkamp L W 2005 *J. Appl. Phys.* **97** 10C506
[38] Wong W C, Ng S M, Wong H F, Mak C L and Leung C W 2017 *IEEE Trans. Magn.* **53** 1–5